J. Fluid Mech. (1990), *vol.* 210, *pp.* 437–458
Printed in Great Britain

Spanwise structure in the near-wall region of a turbulent boundary layer

By R. A. ANTONIA AND D. K. BISSET
Department of Mechanical Engineering, University of Newcastle, NSW, 2308, Australia

(Received 16 January 1989 and in revised form 25 June 1989)

The behaviour of the streamwise velocity u in the near-wall region of a turbulent boundary layer is obtained by analysing the data from an array of hot wires aligned in the spanwise direction. Conventional and conditional statistics are presented, relative to the occurrence of bursts and sweeps detected using a modified u-level method. Sweeps have an average streamwise length which is twice as large as that of bursts while the average spanwise extent of sweeps is about 25% larger than that of bursts. Both instantaneous and conditionally averaged information is presented and discussed in the context of bursts and sweeps in the (x, z)-plane. Dependence on y^+ is significant, and important differences are observed between instantaneous and conditionally averaged results. Conventional and conditional statistics of the velocity derivatives $\partial u/\partial x$ and $\partial u/\partial z$ provide some insight into the anisotropy of the mean-square velocity derivatives in the near-wall region. Conditionally averaged patterns of u compare favourably with the numerical simulations of Kim (1985) in the near-wall region of a turbulent channel flow, at a comparable Reynolds number.

1. Introduction

A significant amount of information has been gathered on various types of coherent structures in a turbulent boundary layer. These structures have different geometries, lengthscales and convection velocities and may differ considerably between one realization and the next. A schematic summary of properties of various structures or their components was given by Cantwell (1981), and Kline (1989) discussed some of the available knowledge of eight classes of quasi-coherent structures in the turbulent boundary layer. In spite of the relatively large body of data now available, a clear idea of how the structures develop and how they are spatially related has not yet emerged.

The fundamental processes are not yet clear even though details of the three-dimensional aspects of structures or flow events associated with structures are now becoming available through large-eddy or direct simulations (e.g. Robinson, Kline & Spalart 1989).

Flow visualization has proved most useful for the identification of events such as bursts (Kline *et al.* 1967), sweeps (Corino & Brodkey 1969) and hairpin vortices (e.g. Head & Bandyopadhyay 1981). In some cases, it has also provided quantitative information on the organized motion. For example, detailed statistics of the spanwise spacing of low-speed streaks have been obtained (Smith & Metzler 1983) using the combination of a hydrogen bubble wire and a high-speed video system.

Compared to flow visualization, the use of multiple hot-wire probes is better for providing quantitative information amenable to statistical analysis. Interesting information on the organized motion has been obtained, both in the near-wall and

outer regions of the boundary layer, from arrays of wires deployed in the (x, y)-plane (e.g. Blackwelder & Kaplan 1976; Brown & Thomas 1977; Antonia, Bisset & Browne 1989). Information has also been obtained from wires deployed in the (x, z)-plane. Gupta, Laufer & Kaplan (1971) studied the spanwise structure of the viscous sublayer by analysing the signals from an array of hot wires which were mounted on a wall plug and aligned in the z (spanwise) direction. Information on the spanwise variation of U, the instantaneous velocity in the streamwise or x-direction, can be used to obtain a pictorial representation of low-speed and high-speed regions (e.g. Blackwelder 1983) by plotting contours of constant U or u (the velocity fluctuation) in t–z coordinates, or x–z coordinates when a space–time transformation is assumed. It is also possible to delineate the relationship, in the (x, z)-plane, between events such as bursts and sweeps (for example, Zaric, Falco & Blackwelder 1984). The experiments of Blackwelder & Swearingen (1989) using z- and y-arrays of hot wires, have confirmed that both $\partial u/\partial z$ and $\partial u/\partial y$ can be as important as $\partial u/\partial x$ and that all gradients play a significant role in the context of an inflectional instability of the wall shear layer.

In the present experiment, a spanwise array of single hot wires is used in the near-wall region of a turbulent boundary layer. The signals from all wires are conditioned on the occurrence of bursts on one of the wires, using the criteria developed and calibrated against flow visualization by Luchik & Tiederman (1987) and Tiederman (1989). Analogous criteria are developed for detecting sweeps. Conventional and conditional correlations between any two signals are examined, particularly for evidence of low-speed streaks in relation to bursts. Properties of bursts and sweeps and the relationship between them in the (x, z)-plane are examined, using both instantaneous realizations and conditional averages at several values of y^+. Because conditional averages based on single-point detections are of necessity symmetrical, further conditions are applied to two of the non-detection wires in order to generate conditional averages of asymmetrical burst regions. Instantaneous and conditionally averaged velocity derivatives $\partial u/\partial x$ and $\partial u/\partial z$ are also examined in relation to bursts, and the strong anisotropy of the near-wall region is noted.

Access to three-dimensional information on the organized motions is possible through either large-eddy or direct simulations (e.g. Kim 1985; Robinson *et al.* 1989) of the Navier–Stokes equations. In general, these simulations permit a finer resolution, with respect to either y or z, than is possible experimentally. A comparison is made between the present conditional averages associated with the end of a burst and those obtained by Kim (1985) from a large-eddy simulation of a turbulent channel flow.

2. Experimental details and conditions

An open-circuit wind tunnel was used in this experiment. The air is supplied from a double inlet centrifugal blower to a diffuser via a flexible coupling. The diffuser is followed by a settling chamber which contains a honeycomb and a number of screens, a two-dimensional (6:1) contraction, and a working section (5.4 m long, 0.89 m high, 0.15 m wide at the entrance). The aerodynamically smooth surface over which the boundary layer develops is vertical and consists of three aluminium plates. The opposite surface of the working section is made up of Perspex panels mounted on a single aluminium frame whose location was adjusted to set up a zero pressure gradient. The boundary layer was tripped with a 1.5 mm dia. rod, located at the beginning ($x = 0$) of the working section, followed by a strip of No. 40 sand paper.

Both the rod and the sand paper spanned the height of the working section. Measurements were made at $x = 4.3$ m and a free-stream velocity U_1 of 4.2 m/s. The Reynolds number $R_\theta \equiv U_1\theta/\nu$, where θ is the momentum thickness, is approximately 2200. At $x = 4.3$ m, the friction velocity U_τ, determined using a Preston tube, is 0.173 m/s and the boundary-layer thickness δ is 0.068 m.

Measurements were made with an array of 10 hot wires aligned in the spanwise direction. The array was mounted on a height gauge which allowed displacement in the y-direction. The hot wires were attached to stainless steel broaches which extend 30 mm upstream of a wedge-shaped support. Wollaston (Pt–10% Rh) wires of diameter $d_w = 2.5$ μm were used. The average (etched) length l_w of the wires was about 0.64 mm and the average (centre to centre) distance Δz between adjacent wires was about 1.35 mm. For the present experiment, the corresponding values of l_w^+ ($\equiv l_w U_\tau/\nu$) and Δz^+ are 7.4 and 15.6 respectively. These values are small enough compared with the expected average wavelength (≈ 100) of low-speed streaks, to resolve information related to low-speed (and presumably high-speed) streaks, although gradients in z could be underestimated. The ratio l_w/d_w (≈ 250) is sufficiently large to minimize end conduction effects.

The hot wires were operated at an overheat of 0.5 with in-house constant-temperature anemometers (see Miller, Shah & Antonia 1987 for details). The output signals were low-pass filtered (cut-off frequency 1750 Hz) before being digitized with a 12 bit sample-and-hold A/D converter at a sampling frequency of 3570 Hz per channel. Data files, each of approximately 40 s duration, were recorded on a PDP 11/34 computer and later transferred to a VAX 8550 computer for the bulk of the data processing.

The hot wires were calibrated in the free stream (at the measurement station) against a Pitot tube connected to a Baratron pressure transducer. The voltage outputs from the transducer and the constant-temperature anemometers were sampled into a personal computer to obtain least-squares estimates of the constants A, B and n in the relation $E^2 = A + BU^n$, where E is the anemometer voltage and U is the mean velocity. The personal computer was also used for simultaneous monitoring of the performance of all wires while the experiment was in progress.

Several basic checks were made to verify that the mean data obtained with the hot-wire array were satisfactory. Values of $\bar{U}$ and a wide range of statistics of u, obtained at all wire locations in the array, validated spanwise homogeneity over the z-range of the array ($z^+ \approx 156$). The y^+ variation of these quantities such as the r.m.s. skewness and flatness factors of u, was in reasonable agreement with available results in the literature. The instantaneous u-signals from all the sensors in the array, located at $y^+ = 15$, are shown in figure 1 for a duration t corresponding to $t^* = 44.3$ or $t^+ = 1430$ (asterisk denotes normalization by U_1 and δ; $t^* = 1$ corresponds to $t^+ = tU_\tau^2/\nu = 32.3$). The most noteworthy feature of the signals is a relatively sudden increase in u, which often follows a gradual decrease in u. The increase in u can sometimes be detected almost simultaneously over nearly the complete z^+ range of the array. This coherence in the z-direction is similar to the coherence of u in the y-direction, observed by Blackwelder & Kaplan (1976) in a region of the layer extending from the wall to $y^+ \approx 100$. The maximum variation in the magnitude of u at $y^+ = 15$ is large. Comparing the signals from all wires, the extreme values of u were about $-7.7U_\tau$ and $10U_\tau$ respectively. The corresponding variation in U is from $0.11U_1$ to $0.84U_1$. For comparison, Blackwelder & Swearingen (1989) reported a $0.2U_1$ to $0.8U_1$ variation for a z-aligned array of hot wires at $y^+ = 15$ and $R_\theta = 2200$.

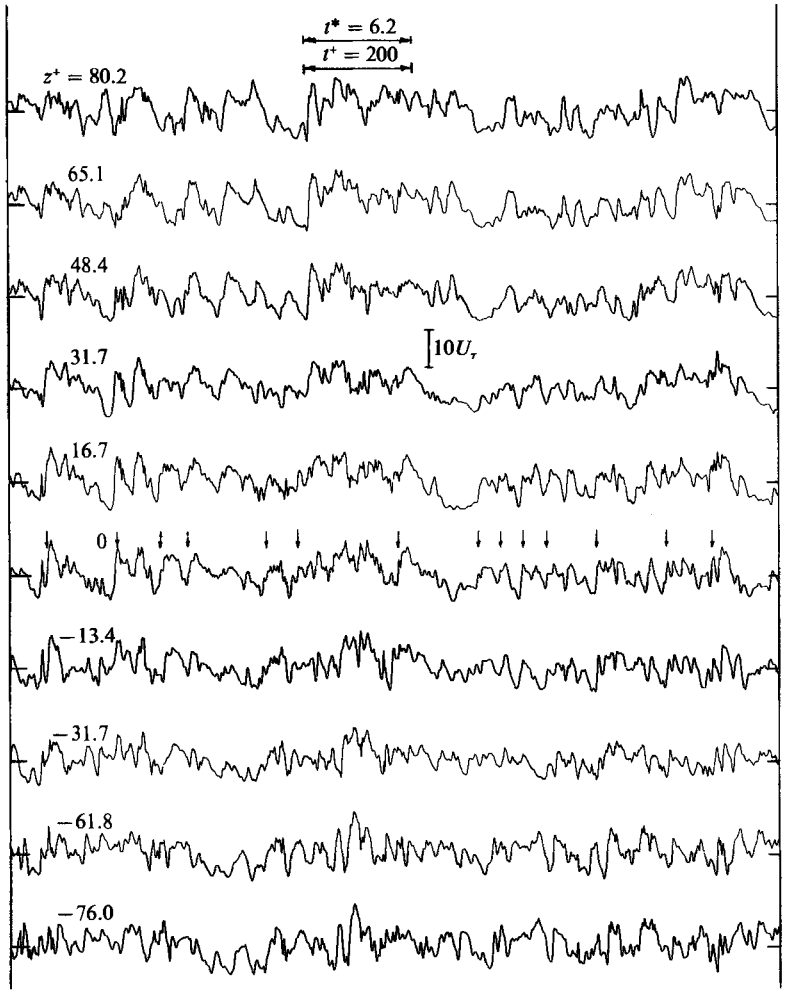

FIGURE 1. Simultaneous velocity signals from the hot-wire array at $y^+ = 15$. Time increases from left to right. The record duration shown is of 0.072 s.

3. Detection of bursts and sweeps

Many methods have been used to detect bursts in the near-wall region of a turbulent boundary layer. It is not the intention here to review these methods; useful references are the paper by Offen & Kline (1975), where various detections were compared with observations from dye slot of visualization, and the papers by Bogard & Tiederman (1986, 1987) which report comparisons between probe detections and flow visualization detections. For the present work, we use a relatively simple detection scheme, based on the measurement of u at a single point in space, as implemented by Luchik & Tiederman (1987) and further refined by Tiederman (1989).

Luchik & Tiederman (1987) modified a scheme, originally introduced by Lu & Willmarth (1973), in which an ejection begins when

$$u < -L\overline{u^2}^{\frac{1}{2}} \tag{1}$$

and ends when

$$u \geqslant -0.25L\overline{u^2}^{\frac{1}{2}}, \tag{2}$$

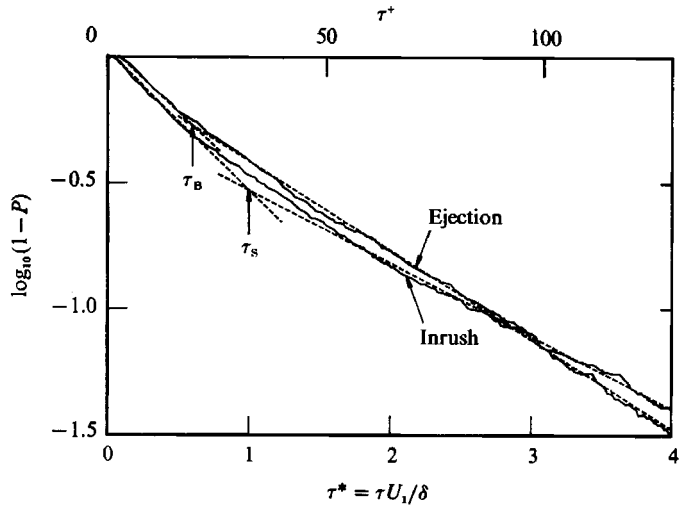

FIGURE 2. Cumulative probability of the time intervals between the end of an ejection (or inrush) and the beginning of the following ejection (or inrush) at $y^+ = 15$.

where L is a threshold parameter. Condition (2) was introduced to eliminate multiple detections of a single ejection. The recognition that consecutive ejections may belong to the same burst has led to several attempts to group ejections. For example, Willmarth & Sharma (1984) switched off the VITA detection criteria for a time equal to the averaging interval to avoid the multiple detection of bursts. The method followed here is that proposed by Barlow & Johnston (1988) and used by Tiederman (1989). The cumulative probability of the time between ejections, as defined by (1) and (2), displays two straight-line portions when plotted on semilogarithmic coordinates, as shown in figure 2. The intersection of the lines defines the grouping time τ_B. Consecutive ejections which are separated by a time smaller than τ_B are considered to belong to the same burst while ejections separated by an interval greater than τ_B are assigned to different bursts. Shah & Antonia (1989) noted that the determination of τ_B is not totally free of ambiguity since there is some subjectivity in fitting the straight-line portions to the probability data. The number of detections depends on τ_B (as reported by Barlow & Johnston 1988), and decreases as τ_B increases. A significant threshold region can be found, however, where the number of detections is practically independent of the threshold parameter (figure 3), thus emphasizing the importance of grouping the ejections from the same burst. The magnitude of $\bar{T}_B$ is reasonably constant in the range $0.2 < L < 0.75$ and increases on either side of this range; this behaviour is similar to that reported by Luchik & Tiederman (1987).

Sweeps, or inrush events, are not as easily identified in flow visualizations as bursts, perhaps because, as noted by Kline (1989), markers introduced near the wall tend to emphasize ejections more than sweeps. Sweeps were first observed over a smooth surface by Corino & Brodkey (1969) (see also Nychas, Hershey & Brodkey 1973). Grass (1971) noted that inrushes, just like ejections, are present irrespective of whether the surface is smooth or rough. Randolph, Eckelmann & Nychas (1987) emphasized that a fourth-quadrant motion ($u > 0$, $v < 0$) description of a sweep (Wallace, Eckelmann & Brodkey 1972) fails to focus on the feature which is characterized by large simultaneous values of $\partial u/\partial t$ and $\partial U/\partial y$. These authors found that, in a fully developed turbulent channel flow, high values of $\partial U/\partial y$ are always

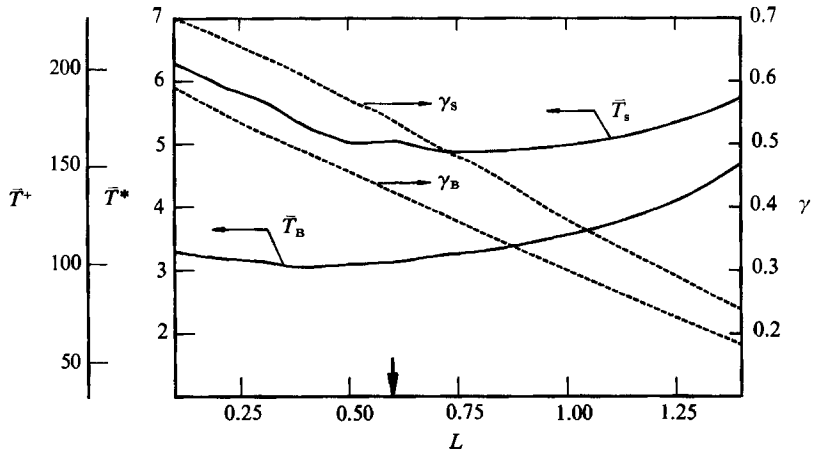

FIGURE 3. Effect of threshold on the normalized average period $\bar{T}^*$ of either bursts or sweeps and on the fraction of time γ occupied by these events at $y^+ = 15$. The final choice of L (for both bursts and sweeps) is indicated by the arrow on the abscissa.

accompanied by large values of $\partial u/\partial t$ in the buffer region ($11 \leqslant y^+ \leqslant 35$). The correlation between $\partial U/\partial y$ and $\partial u/\partial t$ was largest at $y^+ = 15$ when conditioned on values of $\partial U/\partial y$ which are approximately equal to the mean velocity gradient at the wall. There is strong evidence that large simultaneous values of $\partial U/\partial y$ and $\partial u/\partial t$ are associated with strong internal shear layers in the wall zone (Johansson, Alfredsson & Kim 1987*a*). These layers appear to be associated with the lift-up of low-speed fluid from the viscous sublayer and have been observed in experiments (e.g. Johansson *et al* 1987*a*) and in simulations (e.g. Jimenez *et al* 1987; Robinson *et al* 1989). Kline (1989) defines these layers as local regions where the shear rate significantly exceeds its local mean value. Bogard & Tiederman (1987) noted that a strong internal shear layer occurs near the trailing edge of the last ejection in a burst. Although it is plausible that there is a connection between a strong internal shear layer and the arrival of a sweep, a one-to-one correspondence has yet to be established. The VITA algorithm has been used to focus on large positive values of $\partial u/\partial t$, but a method of detecting sweeps directly seems preferable. The definition of a sweep detection presented here cannot be justified as rigorously as that of a burst, however. The burst criterion has evolved from a direct comparison with flow visualization results, but the present sweep criterion is derived by analogy to (1) and (2) without such validation.

The beginning and end of an inrush are defined by

$$u > L\,\overline{u^2}^{\frac{1}{2}} \tag{3}$$

and

$$u \leqslant 0.25L\,\overline{u^2}^{\frac{1}{2}} \tag{4}$$

respectively. Condition (4) was included to avoid the possibility of multiple detections of the same inrush. Grouping of consecutive inrushes was implemented, in similar fashion to the grouping of ejections into bursts, on the assumption that consecutive inrushes can belong to the same sweep. The cumulative probability (figure 2) of the interval between inrushes, exhibits a similar behaviour to that of ejections except that the transition between the two linear segments is wider than for ejections. The magnitude of τ_s, defined by the intersection of the two lines, is larger

than τ_B. The magnitude of $\bar{T}_S$ (figure 3) is correspondingly larger than that of $\bar{T}_B$; the range (0.5 to 1.0) of L for which $\bar{T}_S^*$ is approximately constant is displaced slightly to the right of that for which $\bar{T}_B^*$ is constant. The ejection grouping time τ_B could not be estimated at $y^+ = 5$ (the cumulative probability of the interval between ejections displayed only one straight line) consistent with the fact that bursts have not been observed at such a distance from the wall. The cumulative probability for inrushes, however, still showed the expected behaviour, which gives some support to the use of this method. The fraction of the total time occupied by sweeps, γ_S, is consistently larger (figure 3) than γ_B, and $(\gamma_B + \gamma_S)$ is nearly 1 for the chosen values of $L = 0.6$, $\tau_B^* = 0.6$, and $\tau_S^* = 1.0$. Although the grouping procedure can result in $(\gamma_B + \gamma_S) > 1.0$ when L is small, this is not physically plausible, and therefore L must be $\geqslant 0.55$ for the present data. The results of figure 3 are for $z = 0$, but the variations with z in $\bar{T}^*$ and γ are small (about $\pm 4\%$ for $\bar{T}_S^*$ or $\bar{T}_S^*$ and $\pm 3\%$ for γ_B or γ_S), consistent with the spanwise homogeneity of the mean flow.

The magnitude of $\bar{T}_B^*$ is slightly smaller than that presented in Shah & Antonia (1989) owing to a slightly smaller value of τ_B^* used for the present work. The present value of $\bar{T}_B^*$ (≈ 3.1) is equivalent to $\bar{T}_B^+ = 97$, in reasonable agreement with the measurements of Luchik & Tiederman (1987) and Tiederman (1989) in a duct flow and the numerical simulations of Kim & Spalart (1987) in a boundary layer. Shah & Antonia (1989) found that $\bar{T}_B$ scales on wall variables when $R_d \lesssim 1.5 \times 10^4$ for a fully developed duct flow and when $R_\theta \lesssim 6000$ in a boundary layer. At larger Reynolds numbers, $\bar{T}_B$ was found to scale on mixed or outer variables but this result does not invalidate the law of the wall or the expected scaling of the Reynolds stresses on the wall shear stress in the near-wall region.

The average duration $\bar{T}_S \gamma_S$ of a sweep (= 90 wall units) is about twice as large as the average duration of a burst. The conversion between time- and lengthscales requires the convection velocity of bursts and sweeps to be known. There is only a limited amount of data that are directly relevant; conventional space–time correlation estimates (e.g. Kreplin & Eckelmann 1979) do not distinguish between bursts and sweeps. For a boundary layer over a slightly heated wall, Antonia *et al.* (1988) found that the convection velocity of coolings (sudden decreases in temperature with time at a given x, which coincide with increases in u and which may be associated with sweeps) was slightly larger than that of heatings (which are more likely to be associated with bursts). Johansson *et al.* (1987*a*) obtained a value of $13U_\tau$ for the propagation velocity of the internal shear layer from measurements in a turbulent duct flow. An estimate of $10.6U_\tau$ was reported by Johansson, Alfredsson & Kim (1987*b*) using numerical simulation data for a turbulent duct flow. The previous estimates were found to be approximately independent of y^+ over the near-wall region. In the absence of any definitive results, however, we have assumed that the convection velocity is equal to the local mean velocity $\bar{U}$ (at $y^+ = 15$, $\bar{U} = 10.4U_\tau$) for both bursts and sweeps. With this assumption, the average length of a burst is equal to $\bar{U}\bar{T}_B \gamma_B$, which corresponds to approximately 480 wall units. The average length of a sweep is 960 wall units. It is important to note that the distributions of burst and sweep lengths are highly skewed, with the modes of the distributions being 64 and 83 wall units respectively.

4. Conventional and conditional spanwise correlations of u

The conventional zero-time-delay correlation coefficients ρ_{uu} between the velocity fluctuations at $z = z_0$ and at other points in the array were calculated for $5 \leqslant y^+ \leqslant 40$,

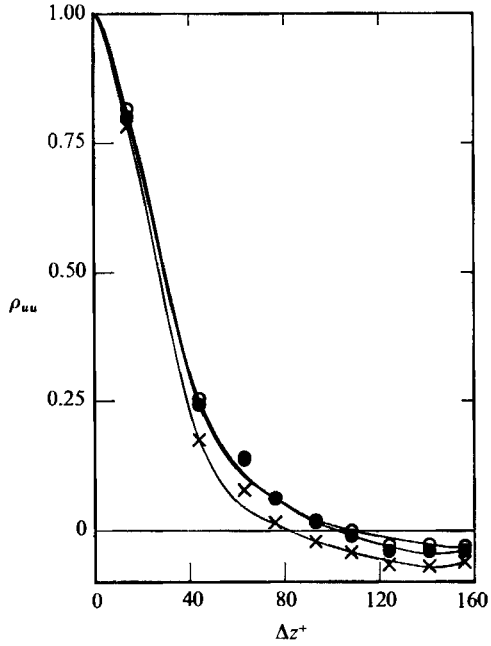

FIGURE 4. Conventional and conditional correlation coefficients of u at $y^+ = 15$. Conditioning is on either bursts or sweeps detected at $z_0^+ = -76$. ●, conventional; ○, sweeps; ×, bursts.

and showed little evidence of periodicity in z that could be related to the sublayer low-speed streaks. Gupta *et al.* (1971), having obtained a similar result, used a short term VITA correlation function to find that 'departures from the observed structures during the averaging time' have a wavelength in z of order $\lambda^+ = 100$ for $y^+ < 8$. In other words, the sublayer streaks are departures from the predominant motion that is responsible for the long-time correlations. In the present work the aim was to determine how ρ_{uu} is affected by the presence of either bursts or sweeps, and therefore the definition of conditional correlation coefficient

$$\rho_{uu}(z) = \frac{\overline{u(z_0)\,u(z)}}{[\overline{u^2(z_0)}\,\overline{u^2(z)}]^{\frac{1}{2}}}$$

was identical to the conventional one except that only the portions of the digital time series in which bursts (or sweeps) were present at $z = z_0$ were used. Note that the mean values of the burst or sweep portions were not subtracted from the fluctuations. The conventional and conditional ρ_{uu} for $z_0^+ = -76$ and $y^+ = 15$ are shown in figure 4. Within the range of z available, the correlation conditioned on bursts is always more negative than the conventional ρ_{uu}, and ρ_{uu} (sweeps) is always marginally more positive. Conditional correlations at several y^+ values are shown in figure 5. Based on the z-values at which the correlations cross zero, the z-scale for sweeps is about 25% greater than that for bursts. The spanwise extent of the conditional correlations increases considerably with y^+ in both cases, and there is no indication of a positive correlation peak at $z^+ - z_0^+ \approx 100$.

Bursting was originally visualized as the lifting and breakup of dye-marked sublayer streaks (Kline *et al.* 1967) which have a mean spacing of $z^+ \approx 100$ (e.g. Smith & Metzler 1983). If bursting had a spanwise wavelength of $z^+ = 100$, it would imply that several adjacent low-speed streaks are often lifted simultaneously while higher

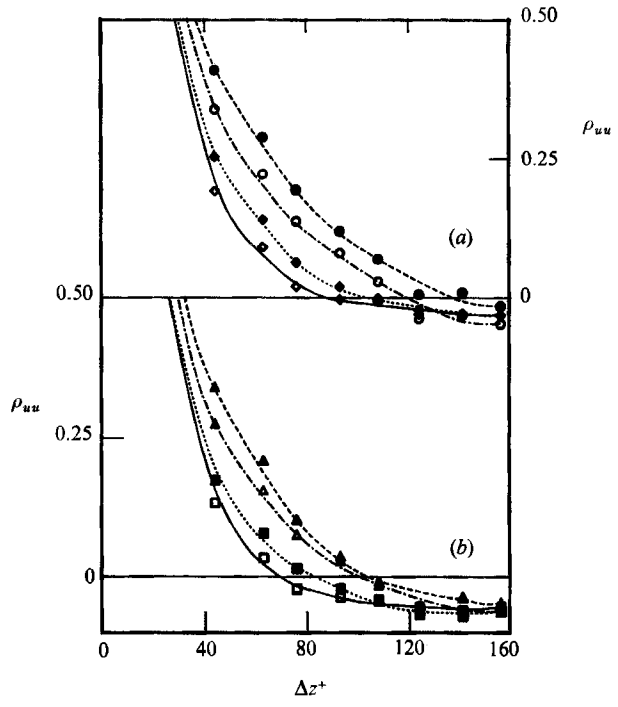

FIGURE 5. Variation through the buffer region of correlation coefficients of u conditioned on either bursts or sweeps detected at $z_0^+ = -76$. Values of y^+ (in order from top to bottom) are 40, 30, 15 and 10. (*a*) Bursts; (*b*) sweeps.

speed fluid descends between them. It is apparent from figure 5(*a*) however, that bursting is part of a process which has a substantially larger spanwise scale than that of the streaks. Results in the following sections provide a more direct (although still incomplete) description of the process.

5. Instantaneous distributions of u

Blackwelder & Swearingen (1989) presented instantaneous profiles of $U(y)$ in a range $0 < y^+ < 100$ and of $U(z)$ at $y^+ = 15$ over a z^+ range of about 200. They drew attention to the inflectional nature of both profiles, pointing out (Blackwelder 1987) that spanwise inflectional profiles occur more often and have a stronger shear than $U(y)$ inflectional profiles. In figure 6, $u(z)$ profiles at $y^+ = 15$ are shown for a duration which is slightly longer than that of one burst. Although the time step between consecutive profiles is $1.08\nu/U_\tau^2$, the time step between consecutive samples is $0.54\nu/U_\tau^2$ (at $y^+ = 15$, at time step of ν/U_τ^2 corresponds to a streamwise step of 10.4 wall units if $\bar{U}$ is taken as the convection velocity). The triangles are the data points; the curve is a spline fit to these points, with continuous first and second derivatives. As in the case of Blackwelder & Swearingen, the spline fit has been differentiated to determine the location ($\mathrm{d}^2u/\mathrm{d}z^2 = 0$) of inflection points shown as solid circles in figure 6(*a*). The first profile in figure 6(*a*) corresponds to the beginning of the burst, and the origin for each profile is displaced to the right by one unit.

The instantaneous profiles display local peaks and valleys, similar to those shown by Blackwelder & Swearingen (1989) and noted by Gupta *et al.* (1971). In figure 6(*a*),

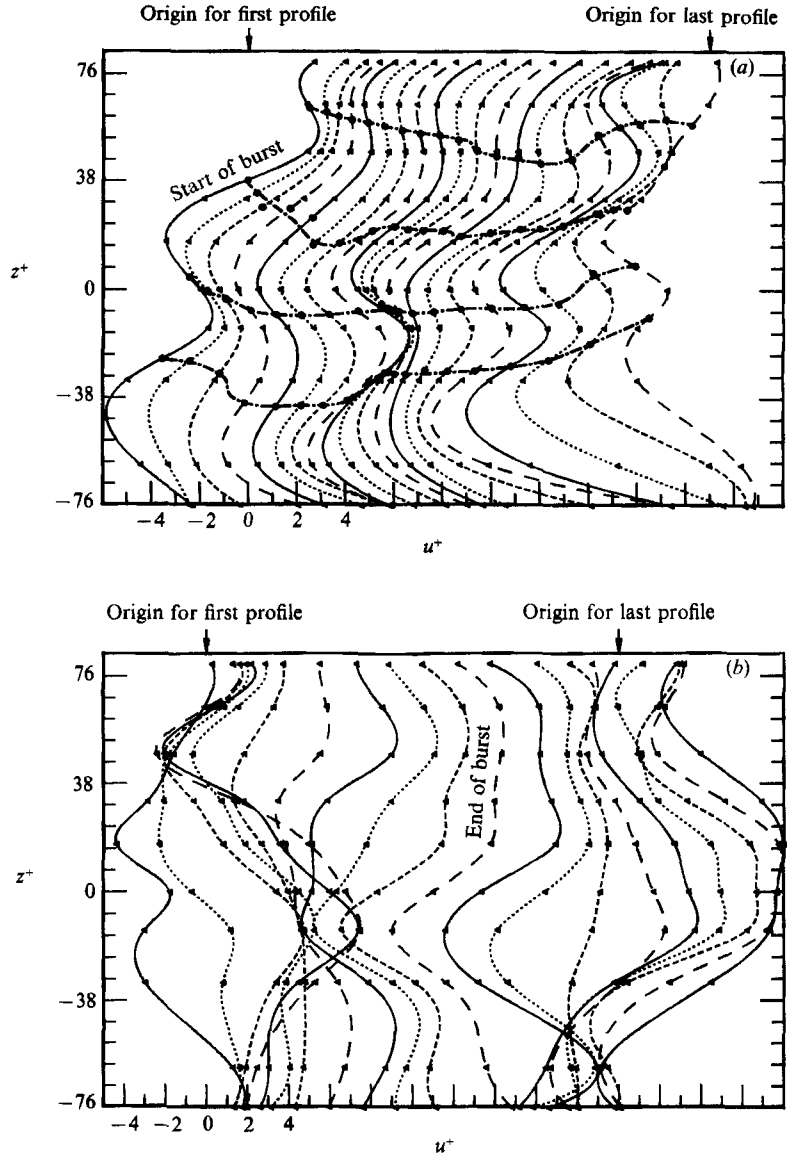

FIGURE 6. Instantaneous profiles in a spanwise direction of the streamwise velocity. The first profile in (*a*) corresponds to the beginning of a burst. The last profile in (*a*) is repeated in (*b*). The time between consecutive profiles is 1.08 wall units. △, data points; ●, points of inflection.

u is mainly negative (even at the locations of local peaks) over a significant central region of the array, with positive values appearing at the edges of the array. The location of a particular peak or valley wanders slightly, in either positive or negative z-directions, as time increases but this spanwise motion is generally well behaved. The previous observation is reasonably well illustrated by the four loci of inflectional points. In particular, the spacing between adjacent loci tends to remain constant during the time span ($\approx$ 20 wall units) covered in figure 6(*a*). For reference, the last profile in figure 6(*a*) is the first profile in figure 6(*b*). The organization of figure 6(*a*) is less evident in figure 6(*b*) especially near the end of the burst. The

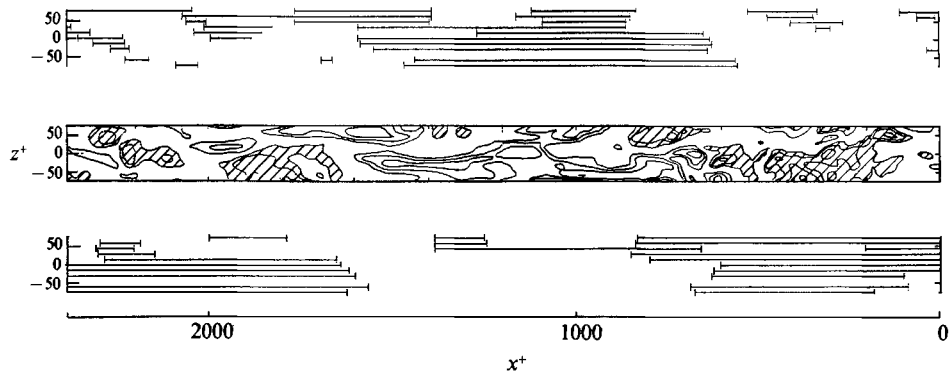

FIGURE 7. Instantaneous contours of u^+ (centre) shown together with detections of bursts (top) and sweeps (bottom) at all wire locations; $y^+ = 15$. Contour values are ± 2.0, ± 3.5 and ± 5.0, with positive contours hatched.

central flow region undergoes a fairly sharp acceleration (for clarity, inflection points are not shown in figure 6*b*) followed by a more gradual deceleration at the end of the burst. Following the end of the burst there is a further acceleration which is less intense but of wider spanwise extent than the acceleration just before the end of the burst. The shape of the $u(z^+)$-distribution (figure 6*b*) near $z^+ = 0$ indicates that the magnitude of $\partial u/\partial z$ can become quite large near the end of the burst. Associated with the large positive acceleration ($\partial u/\partial t > 0$) are large values of $\partial u/\partial z$, negative near $z^+ = 0$ and positive near $z^+ = -20$. The subsequent change of sign in $\partial u/\partial t$ is accompanied by a change of sign in $\partial u/\partial z$. With the assumption that the strong acceleration is also accompanied by a strong shear in the (x, y)-plane, the behaviour of $u(z)$ near the end of the burst implies that the shear layer is strongly three-dimensional in the sense that u changes rapidly in all three directions, as reflected by simultaneously large values of $\partial u/\partial t$ (and hence $\partial u/\partial x$), $\partial u/\partial y$ and $\partial u/\partial z$.

Blackwelder & Swearingen (1989) have noted that inflectional profiles are unstable and that an inviscid two-dimensional instability theory, such as that of Michalke (1965), predicts a streamwise wavelength for the disturbance comparable with that inferred from available results in the near-wall region of a turbulent boundary layer. Although the timescale of the instability is of order ν/U_τ^2, inflectional profiles exist over a time which is larger by at least one order of magnitude. Some support for this is provided by the order of magnitude difference between the timescale for the rapid change in $u(z)$ near the end of the burst in figure 6(*b*) and the persistence time of the inflectional loci in figure 6(*a*).

Contours of the velocity fluctuation u in the (x, z)-plane at $y^+ = 15$, after converting time to distance using $x = -\bar{U}t$, are shown in figure 7 for a duration of 115 ms. Solid lines indicating detections using the algorithms of §3 are shown above (bursts) and below (sweeps) the u-contours. There is close correspondence between negative contours and burst detections, and between positive contours and sweep detections. As expected, there are regions which are not identified as either bursts or sweeps. There is, however, occasional overlap, at the same value of z^+, between bursts and sweeps. This overlap is obviously unrealistic and, as already noted in §3, is a result of the grouping of ejections and inrushes so that $\gamma_B + \gamma_S \approx 1$. Zaric *et al.* (1984), using a different detection method, presented similar figures which also imply that $\gamma_B + \gamma_S$ is not much less than 1. Sweeps can often be seen to follow bursts very closely; statistics for this situation are given in the next section.

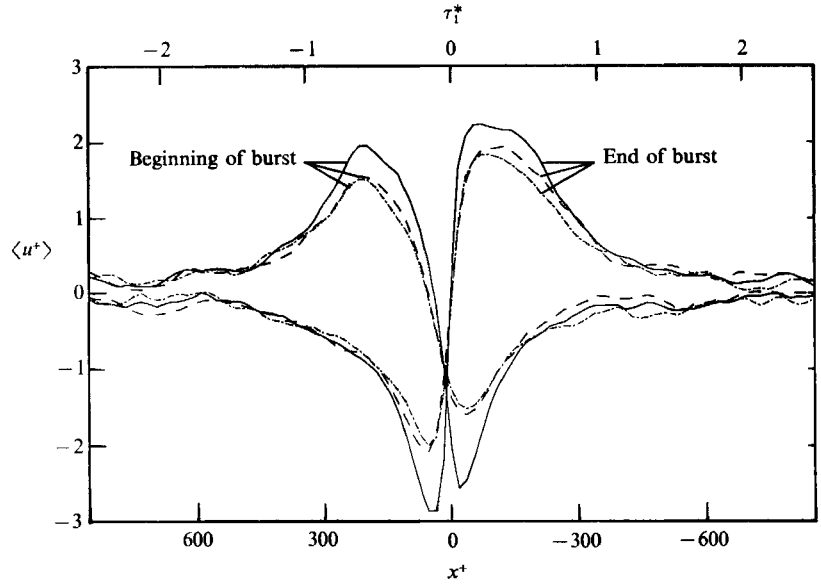

FIGURE 8. Distribution of $\langle u^+ \rangle$ conditioned on either the beginnings or ends of bursts detected at $z^+ = 0$. ——, $z^+ = 16.7$; ——, 0; – – – –, -13.4.

6. Conditionally averaged distributions of u

Averages of u, conditioned on either the beginning or end of bursts (or sweeps), have been calculated in the usual manner, viz.

$$\langle u(\tau_1) \rangle = \frac{1}{N} \sum_{i=1}^{N} u(t_i + \tau_1),$$

where the time τ_1 is measured from the detection instant t_i and N is the total number of detections. All detected bursts or sweeps have been aligned with respect to t_i before averaging is carried out. Distributions of $\langle u \rangle$, corresponding to either the beginning or end of bursts, are shown in figure 8. Those that correspond to either the beginning or end of sweeps are shown in figure 9. Here and in subsequent figures, the time τ_1 has been converted to a distance x with the transformation $x = -\bar{U}\tau_1$; the origin $x = 0$ is therefore the detection location.

It is significant that the positive values of $\langle u \rangle$ in figure 8 are almost as strong as the negative $\langle u \rangle$, given that the detection of bursts is based on negative u only. Also, the decrease in $\langle u \rangle$ at the beginning of a burst is more gradual than the sharp increase in $\langle u \rangle$ at the end of a burst. This increase is consistent with the accelerations that can be observed in the instantaneous traces of figure 1. The arrows in figure 1 indicate the detected locations of the ends of bursts. The difference (figure 8) in the $\langle u \rangle$-distributions between the beginning and end of a burst is consistent with that observed by Wallace, Brodkey & Eckelmann (1977) using a pattern-recognition technique or with that obtained using VITA criteria which focus on positive or negative sudden changes in u or temperature (e.g. Subramanian *et al* 1982; Alfredsson & Johansson, 1984). It is also in close agreement with the difference between the $\langle u \rangle$-distributions of Bogard & Tiederman (1987) conditioned on the initial and last visual contacts of dye ejected from a sublayer streak (and measured with a hot wire). The rapid increase to strongly positive $\langle u \rangle$ at the end of a burst suggests that bursts are usually followed closely by sweeps, whereas the transition

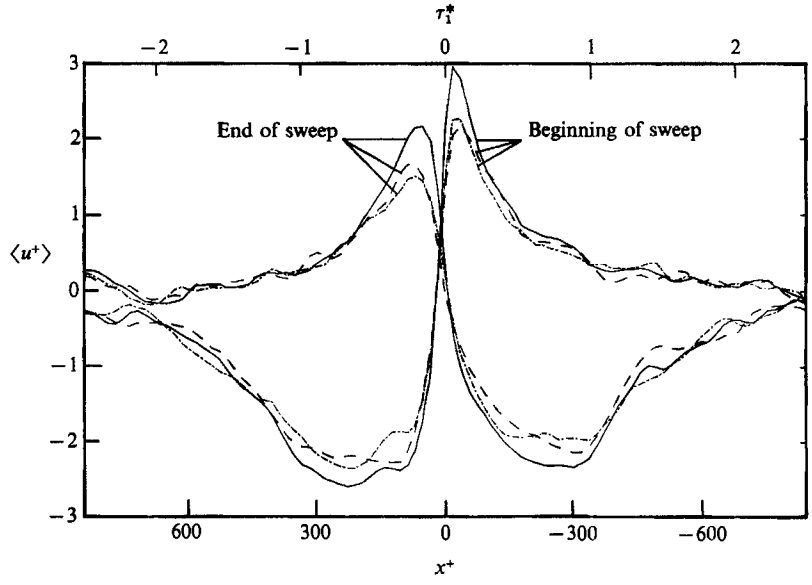

FIGURE 9. Distributions of $\langle u^+ \rangle$ conditioned on either the beginnings or ends of sweeps detected at $z^+ = 0$. ——, $z^+ = 16.7$; ——, 0; – – –, -13.4.

from sweep to burst is not so deterministic. Comparison of figures 8 and 9 indicates a close correlation, at least in the context of $\langle u \rangle$, between the end of a burst and the beginning of a sweep. Since the present condition is imposed at $z^+ = 0$, the $\langle u \rangle$-distributions (figure 8) at either $z^+ = -13.4$ or $z^+ = +16.7$ have a smaller amplitude than at $z^+ = 0$. The $\langle u \rangle$-distributions at $z^+ = -13.4$ and $z^+ = +16.7$ are however nearly identical, consistent with the expected symmetry of $\langle u \rangle$ about $z^+ = 0$.

A more global view of the features exhibited in figures 8 and 9 can be obtained by plotting isocontours of $\langle u \rangle$ in the (x, z)-plane. Such contours are shown in figure 10(*a*) where conditioning is with respect to the beginning and end of a burst and in figure 11 where conditioning is on the beginning and end of a sweep. The condition was applied at $z^+ = 0$ (results not shown) and near the edge of the array ($z^+ = 65$). Since contours are symmetrical about the detection location, the contours conditioned at $z^+ = 65$ are shown here as they provide a larger z^+ range. As could be expected from the correlations of figure 5, the organizing effect of detection at one point extends to a considerable distance in z. Figure 10(*a*) shows that for $x^+ < 0$, i.e. upstream of the beginning of a burst, negative $\langle u \rangle$-contours are flanked by shorter positive $\langle u \rangle$-contours. For $x^+ > 0$, this pattern is reversed, and the main positive $\langle u \rangle$-regions are now flanked by negative $\langle u \rangle$-regions. Both streamwise and spanwise dimensions of the main low-speed and high-speed regions show substantial increases with y^+. A noticeable difference between figures 10(*b*) and 10(*a*) is the concentration of the contours near $x^+ = 0$ in figure 10(*b*), underlining the strong gradient of u which accompanies the end of a burst (figure 8). The same concentration is also present in figure 11(*a*), beginning of sweep. In order to quantify the correspondence between the beginning of a sweep and the end of a burst, the number of detection instants for these two events that occurred within a certain window was counted. The window was set to a duration of ± 5 wall units (or a distance of ± 52 wall units) comparable to Johansson *et al*'s (1987*a*) estimate of about 100 wall units for the streamwise extent of the internal shear layer. With this window, 51% of the detections

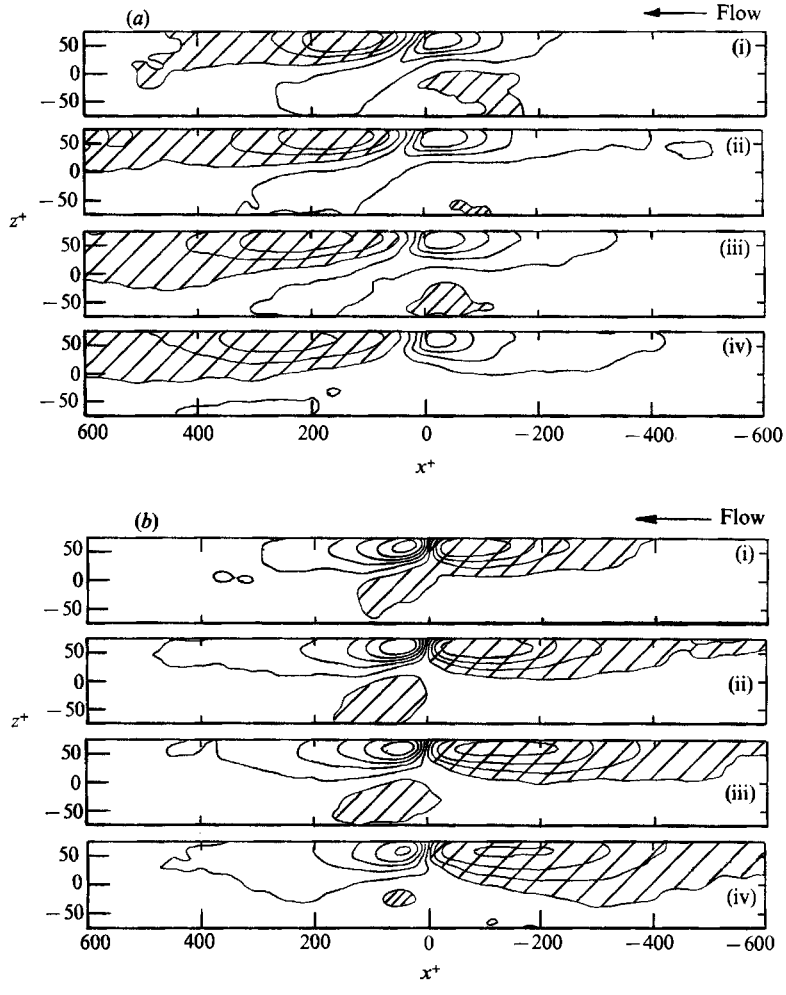

FIGURE 10. Contours of $\langle u^+ \rangle$ conditioned on either the beginnings or ends of bursts detected at $z^+ = 65$. Positive contours are hatched. The contour increment is 0.5. (*a*) Beginning of burst: (i) $y^+ = 10$; (ii) 15; (iii) 30; (iv) 40. Minimum and maximum contours are -1.75 and 1.25 respectively. (*b*) End of burst: (i) $y^+ = 10$; (ii) 15; (iii) 30; (iv) 40. Minimum and maximum contours are -2.25 and 1.75 respectively.

identifying the beginnings of sweeps matched those identifying the ends of bursts. The matching between beginning of burst detections and end of sweep detections was only 28%. Both bursts and sweeps are quasi-periodic in time, and therefore one must follow the other in general, but the implication here is that the combination of burst, shear layer, and sweep are closely related in that temporal order, not the reverse.

It should be underlined that the patterns in figures 10 and 11 are conditional averages and may not be present instantaneously. A particular detection procedure may detect structures that are aligned differently in space without distinguishing them, and therefore some potentially useful information may be lost in the averaging. To demonstrate this, some addtional criteria were applied to the end-of-burst detections previously obtained at $y^+ = 15$ and $z^+ = 0$. Defining $\bar{u}$ as the average value of u for $-100 \leqslant x^+ \leqslant 100$ relative to each detection, the detections were divided into four subgroups according to whether $\bar{u}$ was positive or negative at either

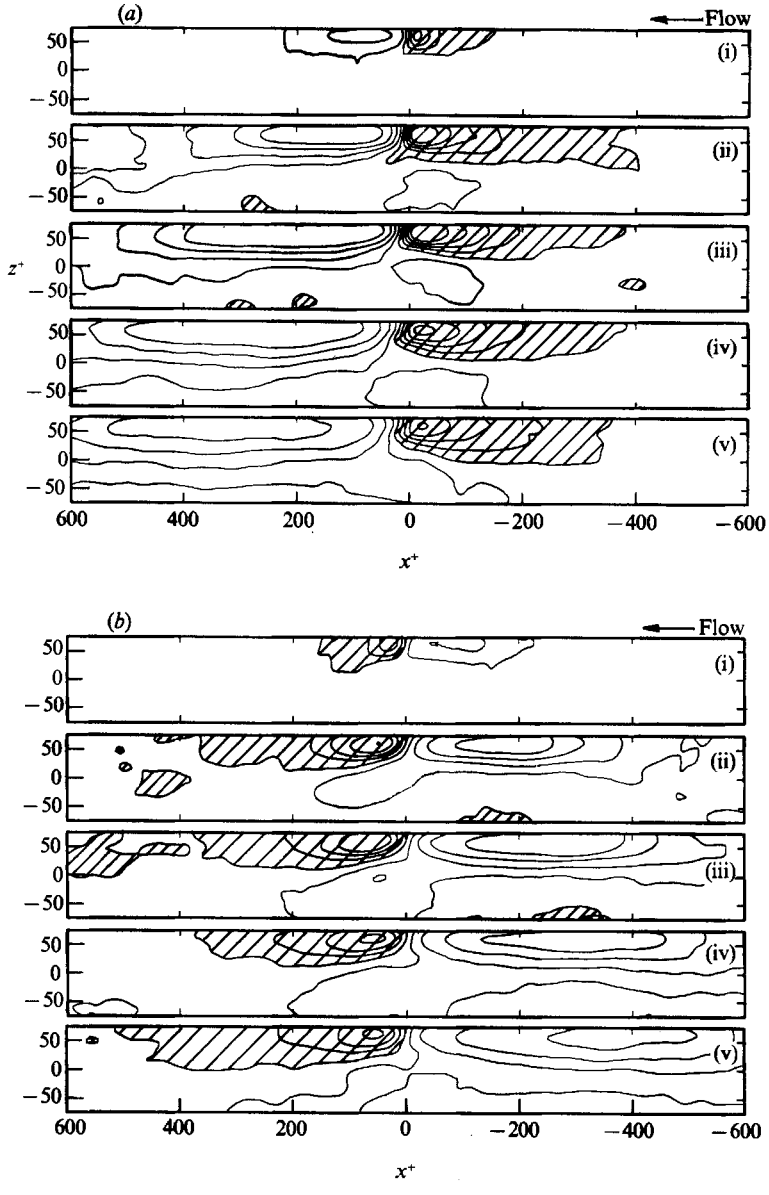

FIGURE 11. Contours of $\langle u^+ \rangle$ conditioned on either the beginnings or ends of sweeps detected at $z^+ = 65$. Positive contours are hatched. The contour increment is 0.5. (*a*) Beginning of sweep: (i) $y^+ = 5$; (ii) 10; (iii) 15; (iv) 30; (v) 40. Minimum and maximum contours are -1.75 and 2.25 respectively, except for (i) where they are -0.75 and 1.75. (*b*) End of sweep: (i) $y^+ = 5$; (ii) 10; (iii) 15; (iv) 30; (v) 40. Minimum and maximum contours are -1.75 and 1.75 respectively, except for (i) where they are -0.75 and 1.25.

or both of the locations $z^+ = -76$ and $z^+ = 80$. The subgroups each contained about 25% of the detections, consistent with the very low value of ρ_{uu} at $|\Delta z^+| \approx 80$ (figure 4). The resulting contours of $\langle u \rangle$, figure 12, represent most of the main characteristics found in the u-contours for individual detections: isolated low-speed regions (figure 12*a*), isolated high-speed regions (figure 12*d*), and regions where contours are slewed or kinked (figures 12*b*, 12*c*) With the z^+ origins displaced appropriately, the

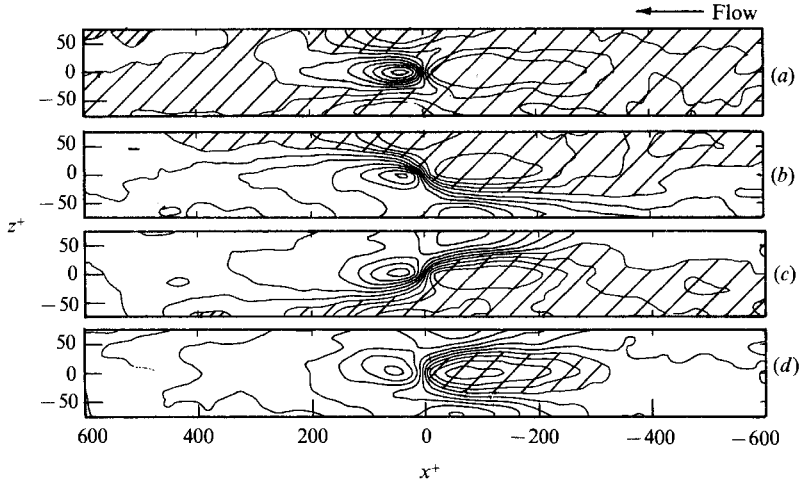

FIGURE 12. Contours of $\langle u^+ \rangle$ conditioned on the end of a burst detected at $z^+ = 0$ and $y^+ = 15$, with the additional requirements that $\bar{u}$ (see text) is either positive or negative at $z^+ = 80$ and $z^+ = -76$. (*a*) $\bar{u} > 0$ ($z^+ = 80$) and $\bar{u} > 0$ ($z^+ = -76$); (*b*) $\bar{u} > 0$ and $\bar{u} < 0$; (*c*) $\bar{u} < 0$ and $\bar{u} > 0$; (*d*) $\bar{u} < 0$ and $\bar{u} < 0$. Contour increment is 0.5 and range -2.75 to $+1.75$, and positive contours are hatched.

contours of figure 10*b*(ii) are the average of the parts of figure 12, just as the correlations of figure 5 represent averages of the contours of figures 10 and 11. The contours of figure 12(*a*) are consistent with the idea of bursting as the lifting of low-speed fluid between the legs of a hairpin vortex, but they represent only one quarter of all bursts.

In the context of numerical simulations of the near-wall region of turbulent channel and boundary-layer flows, Johansson *et al.* (1987*b*) noted that instantaneous u-patterns in the (x, y)-plane often exhibit strong asymmetries (about the z-coordinate) which disappear after ensemble averaging†. To obtain asymmetry in the ensemble-averaged patterns, the z-coordinate was switched according to the sign of $\partial u/\partial z$ at the detection point. Their resulting contours are rather similar to those of figure 12(*b*).

There is no *a priori* reason why bursting – the lifting and breakup of sublayer streaks – should have the same z^+ scale as the streaks themselves. The width of low-speed regions conditioned on bursting and the z^+ distance to the centres of the adjacent high-speed regions (figure 10) indicate that the bursting process has a z^+ scale at least two or three times larger than that of the streaks (at the present Reynolds number). This is consistent with both conditional correlation coefficients (figures 4 and 5) and the nature of instantaneous burst detection regions (e.g. figure 7). It is not possible to say from this whether bursting is initiated within the sublayer or at a greater height, however.

7. Velocity derivatives: statistics and conditioning

As noted earlier, Randolph *et al.* (1987) carried out a systematic study throughout the buffer region of the correlation between $\partial u/\partial t$ and $\partial U/\partial y$. The main motivation of their study was to provide an effective criterion for the onset of the sweep. The correlation coefficient between $\partial u/\partial t$ and $\partial U/\partial y$ was large at $y^+ = 15$, especially when

† Differences, in the (y, z)-plane, between instantaneous and conditional patterns have also been reported by Guezennec, Piomelli & Kim (1987).

conditioned on values of $\partial U/\partial y$ that were comparable to the velocity gradient at the wall. In this section, conventional and conditional data are presented for $\partial u/\partial x$ and $\partial u/\partial z$. The derivative $\partial u/\partial x$ was inferred using Taylor's hypothesis from $\partial u/\partial t$. In the calculation of $\partial u/\partial t$ a time step of one sampling interval was used, which corresponds to a step in x^+ of 5.6. The derivative $\partial u/\partial z$ was approximated by the ratio $\Delta u/\Delta z$, where Δu is the difference between values of u at neighbouring sensors in the array, and Δz is the separation between these sensors. The value of $\partial u/\partial z$ was assigned to a point midway between neighbouring hot wires, and the average value of Δz^+ is 15.6 (for Blackwelder & Swearingen's 1989 boundary-layer measurements at $R_\theta = 2200$, Δz^+ was about 20). The influence of the magnitudes of Δx^+ and Δz^+ on the r.m.s. values of the derivatives was tested, first by using a higher-order expression for the derivative, and then by varying the size of Δx^+ and Δz^+. Because Δz^+ was not identical for all pairs of hot wires, precluding a simple form of high-order derivative, a cubic equation in u^+ was fitted to the values from a group of four adjacent wires, and differentiated at the midpoint of the group. (This procedure is similar to the spline fitting used in figure 6.) The effect on r.m.s. values of $\partial u^+/\partial z^+$ was quite small, i.e. an average increase of about 5% compared to results with the simple derivative. The effect on the r.m.s. value of $\partial u^+/\partial x^+$ of applying the same procedure to four values of u^+ (adjacent in time and therefore in x) was negligible. Still using the cubic fit, Δx^+ was increased by factors of 2, 3, 4, 8 and 16 and the r.m.s. of $\partial u^+/\partial x^+$ showed an almost linear decrease. Extrapolation to $\Delta x^+ = 0$ implied an error of at most 2% in $\overline{(\partial u^+/\partial x^+)^2}^{\frac{1}{2}}$ *for* $\Delta x^+ = 5.6$ and 7% for $\Delta x^+ = 15.6$. When Δz^+ was increased by a factor of 2, the r.m.s. of $\partial u^+/\partial z^+$ decreased in an approximately similar manner to that of $\partial u^+/\partial x^+$, implying that, for $\Delta z^+ = 15.6$, $\overline{(\partial u^+/\partial z^+)^2}^{\frac{1}{2}}$ is underestimated by roughly 7%.

There are significant differences between the probability density function (p.d.f.) of $\partial u/\partial x$ and that of $\partial u/\partial z$. A semilogarithmic presentation is used in figure 13 to emphasize the different behaviours between the positive and negative tails of the p.d.f. The p.d.f. of $\partial u/\partial z$ is essentially symmetrical although non-Gaussian (the flatness factor is about 3.8). By contrast, the skewness of $\partial u/\partial x$ is about -1, as reflected by the negative tail of the p.d.f. of $\partial u/\partial x$ (figure 13), and the flatness factor is about 8. Although the peak positive and negative values of $\partial u/\partial z$ are likely to be attenuated as a result of the wire length and the separation between wires, the minimum and maximum values of $\partial u^+/\partial z^+$ were approximately -0.8 and 0.8 at $y^+ = 15$, indicating that extrema in the spanwise shear are comparable to the wall shear. Randolph *et al.* (1987) found that, at $y^+ = 15$, the maximum value of $\partial U^+/\partial y^+$ is close to one. The present results at $y^+ = 15$ provide quantitative support for Blackwelder & Swearingen's (1989) observation that extrema in $\partial u/\partial z$ are as important as those in $\partial U/\partial y$.

The conventional r.m.s. value of $\partial u^+/\partial x^+$ at $y^+ = 15$ was found to be 0.059 with negligible variation for all hot wires of the array. The average value of the conventional r.m.s. of $\partial u^+/\partial z^+$ was 0.125, but there was a variation (up to $\pm 20\%$) in the values obtained from the various pairs of hot wires, due in part to uncertainty in the measurement of Δz^+. Linear extrapolation to $\Delta z^+ = 0$ would increase the r.m.s. value by 7% to 0.134. The ratio of variances, i.e. $\overline{(\partial u^+/\partial z^+)^2}/\overline{(\partial u^+/\partial x^+)^2}$, is in the range 4.5 to 5.0, more than twice as large as the isotropic value of 2. The extent of the anisotropy underlines the relatively large values of $\partial u/\partial z$ which can arise as a result of the organized motion near the wall. One would expect that $\overline{(\partial u/\partial y)^2}$ would be slightly larger than $\overline{(\partial u/\partial z)^2}$ by reference to the relative magnitudes of $\overline{(\partial\theta/\partial x)^2}$, $\overline{(\partial\theta/\partial y)^2}$ and $\overline{(\partial\theta/\partial z)^2}$ (θ is the temperature fluctuation) obtained by Krishnamoorthy

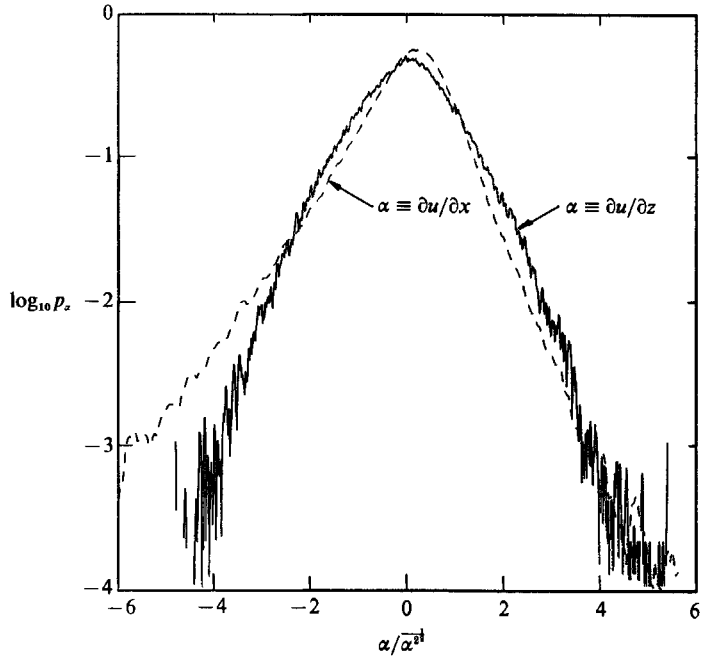

FIGURE 13. Probability density functions of $\partial u/\partial x$ (---) and $\partial u/\partial z$ (——) at $y^+ = 15$.

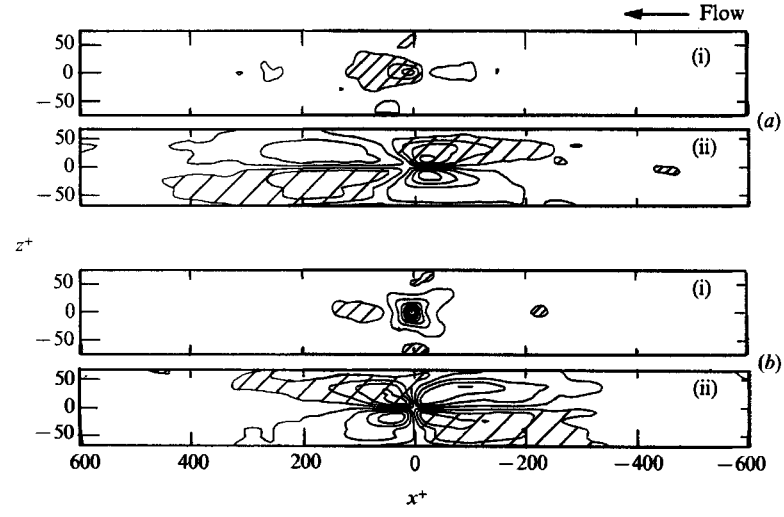

FIGURE 14. Contours of $\partial\langle u^+\rangle/\partial x^+$ and $\partial\langle u^+\rangle/\partial z^+$ near the beginning and end of a burst at $y^+ = 15$. (*a*) Beginning of burst: (i) $\partial\langle u^+\rangle/\partial x^+$; (ii) $\partial\langle u^+\rangle/\partial z^+$. (*b*) End of burst: (i) $\partial\langle u^+\rangle/\partial x^+$; (ii) $\partial\langle u^+\rangle/\partial z^+$. Contour increment is 0.02 and range −0.15 to 0.07, and positive contours are hatched.

& Antonia (1987) in a turbulent boundary layer over a slightly heated wall. Near $y^+ = 15$, $\overline{(\partial\theta/\partial y)^2} \approx 2\overline{(\partial\theta/\partial z)^2}$ and $\overline{(\partial\theta/\partial z)^2} \approx 7\overline{(\partial\theta/\partial x)^2}$.

Patterns of $\partial\langle u^+\rangle/\partial z^+$ and $\partial\langle u^+\rangle/\partial x^+$ conditioned on the beginning of a burst at $z^+ = 0$ (figure 14*a*) are qualitatively similar to those conditioned on the end of a burst (figure 14*b*), although quantitative differences exist. It should first be noted that $\partial\langle u\rangle/\partial x$ should be symmetrical about $z = 0$ whereas $\partial\langle u\rangle/\partial z$ should be anti-symmetrical with respect to z, as shown in figure 14. While the $\partial\langle u^+\rangle/\partial x^+$ contours

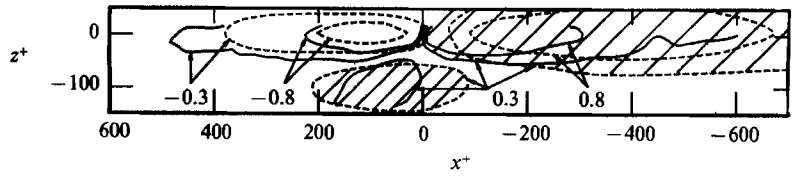

FIGURE 15. Comparison between the present $\langle u^+ \rangle$ contours conditioned on the end of a burst at $y^+ = 15$ (see figure 10*b*(ii)) and those of Kim (1985). Positive contours are hatched. ——, Present; ——, Kim (1985).

occur within a narrow region of x^+, especially near the end of a burst, the $\partial\langle u^+\rangle/\partial z^+$ contours are elongated, the elongation appearing more pronounced before the beginning and after the end of a burst. When considered together, figures 14(*a*) and 14(*b*) indicate that, in the interval between the beginning and end of a burst, $\partial\langle u^+\rangle/\partial z^+$ is essentially positive for $z^+ > 0$ and negative for $z^+ < 0$. In figure 14*b* (ii), the change in sign of $\partial\langle u^+\rangle/\partial z^+$ occurs almost exactly at the detection location, whereas in figure 14*a* (ii) it occurs slightly downstream of the beginning of the burst. Contour values of $\partial\langle u^+\rangle/\partial z^+$ are the same near the beginning of a burst and near the end of a burst whereas much larger magnitudes of $\partial\langle u^+\rangle/\partial x^+$ occur near the end of the burst. The maximum value of $\partial\langle u^+\rangle/\partial x^+$ is twice as large as that of $\partial\langle u^+\rangle/\partial z^+$. The distributions of $\partial u^+/\partial x^+$ and $\partial u^+/\partial z^+$ that may be inferred from instantaneous u^+ profiles (figure 6) or contours (figure 7) often differ significantly from the conditionally averaged gradients (figure 14), but the general pattern (localized extrema in $\partial u^+/\partial x^+$ and longitudinally extended regions of large $\partial u^+/\partial z^+$) is maintained.

8. Comparison with numerical simulations

A number of results have now been obtained from numerical simulations in wall turbulent shear flows. In the present context, it is useful to compare the present $\langle u \rangle$-contours with those obtained by Kim (1985) in the near-wall region of a fully developed turbulent channel flow. In Kim's large-eddy simulation data, the Reynolds number was about 1.4×10^4 (based on centreline velocity and half-channel width) and grid spacings of 62 and 15 were used for x^+ and z^+. In the present experiment, the Reynolds number based on U_1 and the boundary-layer thickness is equal to 1.9×10^4 while the streamwise and spanwise spacings for the data were 5.4 and 15.7 wall units. Kim used a variable-interval space averaging or VISA technique for detecting the bursting event. This technique (essentially the spatial equivalent of VITA) was used with $k = 1.2$ and a spatial averaging length of 500 wall units. One of the criteria used was the inequality $\partial u/\partial x < 0$ so that the technique focused on the end of the burst. Kim's contours should therefore be comparable to those in figure 10(*b*). A few contours from part of figure 11 of Kim's (1985) paper have been selected and are shown in figure 15 with similar contour values obtained for the present experiment. The figure indicates that, in both experiment and simulation, the length of the central positive contour is larger than that of the negative contour. Similarly, the spanwise extent of the positive region is larger than that of the negative region, the difference being more marked in the simulation than in the experiment. There is good agreement, between simulation and experiment, in the characteristics of the positive contours below $z^+ = 0$. The maximum value of $\partial u/\partial x$ appears to be larger in the experiment than in the simulation, reflecting the relatively coarse streamwise grid spacing in the simulation.

On the basis of $\langle u \rangle$-contours in both the (x, y)- and (x, z)-planes, Kim (1985) concluded that the low-speed region is completely surrounded by high-speed fluid. The interface at the end of the burst between low- and high-speed fluid would then form a three-dimensional shear layer containing significant vorticity. This description is applicable strictly in a conditionally averaged sense since, as has been noted earlier, individual realizations may not contain features that are observed at a conditionally averaged level. Using contours of ensemble-averaged spanwise vorticity in the (y, z)-plane, Kim inferred the existence near the wall of a horseshoe-type vortex underneath the sweeping motion. The present contours of $\partial\langle u \rangle/\partial z$ in the (x, y)-plane are not inconsistent with this description, although $\partial\langle u \rangle/\partial z$ represents only part of $\langle \omega_y \rangle$, the averaged y-vorticity component. Since $\partial\langle u^+ \rangle/\partial z$ is antisymmetrical about $z = 0$, it may be argued that the hairpin vortex, with perfectly antisymmetrical distributions of $\langle \omega_y \rangle$ (or $\langle \omega_x \rangle$) about $z = 0$, is an artifact of conditional averaging. Instantaneously, such hairpin vortices may occur only rarely (e.g. Robinson *et al.* 1989) but there is sufficient evidence, in both flow visualizations and numerical simulations, to support the existence of such vortices or parts of such vortices that are undergoing substantial distortion in various ways.

9. Conclusions

A spanwise array of hot wires has been used in combination with methods of detecting bursts and sweeps to provide information on the spanwise structure of u in the near-wall region of a turbulent boundary layer. Both instantaneous and conditionally averaged velocity patterns in the (x, z)-plane have been obtained, with conditioning on the occurrence of bursts and sweeps.

The data indicate that the average streamwise length of a sweep (≈ 960 wall units at $y^+ = 15$) is about twice as large as that of a burst. The spanwise extent of a sweep, determined from conditional correlations of u, is larger, by about 25%, than that of a burst. The streamwise length and spanwise extent of bursts and sweeps were found to increase with distance from the wall. Conditional correlations, contours of $\langle u \rangle$, and instantaneous burst detections all imply that the motion associated with bursting has a spanwise scale considerably larger than that of the sublayer low-speed streaks.

Contours of $\langle u \rangle$ based on single-point detections, of necessity symmetrical about the detection plane, confirm that the organized motion extends for considerable distance in both x and z. There are large off-axis differences between individual realizations of bursts or sweeps, however. The initial set of end-of-burst detections was divided into four groups according to whether the average values of u for $-100 < x^+ < 100$ relative to each detection, at either or both of $z^+ = -76$ and $z^+ = 80$, were positive or negative, and the resulting contours of $\langle u \rangle$ accounted for some of the important off-axis differences including asymmetry.

There is reasonable agreement between the present $\langle u \rangle$-contours near the end of a burst and those obtained by Kim (1985) from a numerical simulation in a turbulent channel flow. Contours of $\langle u \rangle$ and especially $\partial\langle u \rangle/\partial x$ and $\partial\langle u \rangle/\partial z$ highlight the presence of the three-dimensional internal shear layer which is associated with the end of a burst and marks, with reasonable probability, the interface between a burst and a sweep. The largest values of $\partial\langle u \rangle/\partial x$ occur at this interface and the largest values of $\partial\langle u \rangle/\partial z$ occur in the vicinity of the interface. Whereas large streamwise gradients of $\langle u \rangle$ occur in relatively concentrated regions of space, large spanwise derivatives of $\langle u \rangle$ are spread over significant streamwise distances. These

observations may explain the inequality $\overline{(\partial u/\partial z)^2} > \overline{2(\partial u/\partial x)^2}$, which reflects the strong anisotropy near the wall. They are also consistent with the expected zero average correlation between $\partial u/\partial x$ and $\partial u/\partial z$. Instantaneously, the product of $\partial u/\partial x$ and $\partial u/\partial z$ can be large and of either sign. The largest magnitude of $\partial u/\partial z$ is comparable with that of the mean velocity gradient at the wall.

The support of the Australian Research Council is gratefully acknowledged. The authors are grateful to Drs D. A. Shah and L. V. Krishnamoorthy for their contributions to the experiments.

REFERENCES

ALFREDSSON, P. H. & JOHANSSON, A. Y. 1984 On the detection of turbulence-generating events. *J. Fluid Mech.* **139**, 325–345.

ANTONIA, R. A., BISSET, D. K. & BROWNE, L. W. B. 1989 Effect of Reynolds number on the organised motion in a turbulent boundary layer. *Proc. Zaric Memorial Intl Seminar on Near-Wall Turbulence*. Hemisphere (to appear).

ANTONIA, R. A., FULACHIER, L., KRISHNAMOORTHY, L. V., BENABID, T. & ANSELMET, F. 1988 Influence of wall suction on the organised motion in a turbulent boundary layer. *J. Fluid Mech.* **190**, 217–240.

BARLOW, R. S. & JOHNSTON, J. P. 1988 Local effects of large-scale eddies on bursting in a concave boundary layer. *J. Fluid Mech.* **191**, 177–195.

BLACKWELDER, R. F. 1983 Analogies between transitional and turbulent boundary layers. *Phys. Fluids* **26**, 2807–2815.

BLACKWELDER, R. F. 1987 Coherent structures associated with turbulent transport. In *Phenomena in Turbulent Flows: Theory, Experiment and Numerical Simulation* (ed. M. Hirata & N. Kasagi). Hemisphere.

BLACKWELDER, R. F. & KAPLAN, R. E. 1976 On the bursting phenomenon near the wall in bounded turbulent shear flows. *J. Fluid Mech.* **76**, 89–112.

BLACKWELDER, R. F. & SWEARINGEN, J. D. 1989 The role of inflectional velocity profiles in wall bounded flows. *Proc. Zaric Memorial Intl Seminar on Near-Wall Turbulence*. Hemisphere (to appear).

BOGARD, D. G. & TIEDERMAN, W. G. 1986 Burst detection with single-point velocity measurements. *J. Fluid Mech.* **162**, 389–413.

BOGARD, D. G. & TIEDERMAN, W. G. 1987 Characteristics of ejections in turbulent channel flow. *J. Fluid Mech.* **179**, 1–19.

BROWN, G. L. & THOMAS, A. S. W. 1977 Large structure in a turbulent boundary layer. *Phys. Fluids* **20**, S243–S252.

CANTWELL, B. J. 1981 Organized motion in turbulent flow. *Ann. Rev. Fluid Mech.* **13**, 457–515.

CORINO, E. R. & BRODKEY, R. S. 1969 A visual investigation of the wall region in turbulent flow. *J. Fluid Mech.* **37**, 1–30.

GRASS, A. J. 1971 Structural features of turbulent flow over smooth and rough boundaries. *J. Fluid Mech.* **50**, 233–256.

GUEZENNEC, Y. G., PIOMELLI, U. & KIM, J. 1987 Conditionally-averaged structures in wall-bounded turbulent flows. In *Proc. 1987 Summer Program of the NASA-Stanford Center for Turbulence Research*, CTR-S87, pp. 263–272.

GUPTA, A. K., LAUFER, J. & KAPLAN, R. E. 1971 Spatial structure in the viscous sublayer. *J. Fluid Mech.* **50**, 493–512.

HEAD, M. R. & BANDYOPADHYAY, P. 1981 New aspects of turbulent boundary-layer structure. *J. Fluid Mech.* **107**, 297–388.

JIMENEZ, J., MOIN, P., MOSER, R. D. & KEEFE, L. R. 1987 Ejection mechanisms in the sublayer of a turbulent channel. In *Proc. 1987 Summer Program of the NASA-Stanford Center for Turbulence Research*, CTR-S87, pp. 37–47.

JOHANSSON, A. V., ALFREDSSON, P. H. & ECKELMANN, H. 1987*a* On the evolution of shear-layer structures in near-wall turbulence. In *Advances in Turbulence* (ed. G. Comte-Bellot & J. Mathieu), pp. 383–390. Springer.

JOHANSSON, A. V., ALFREDSSON, P. H. & KIM, J. 1987*b* Shear-layer structures in near-wall turbulence. In *Proc. 1987 Summer Program of the NASA-Stanford Center for Turbulence Research* CTR-S87, pp. 237–251.

KIM, J. 1985 Turbulence structures associated with the bursting event. *Phys. Fluids* **28**, 52–58.

KIM, J. & SPALART, P. R. 1987 Scaling of the bursting frequency in turbulent boundary layers at low Reynolds numbers. *Phys. Fluids* **30**, 3326–3328.

KLINE, S. J. 1989 Quasi-coherent structures in the turbulent boundary layer. Part I: Status report on a community-wide summary of the data. *Proc. Zaric Memorial Intl Seminar on Near-Wall Turbulence*. Hemisphere (to appear).

KLINE, S. J., REYNOLDS, W. C., SCHRAUB, F. A. & RUNSTADLER, P. W. 1967 The structure of turbulent boundary layers. *J. Fluid Mech.* **30**, 741–773.

KREPLIN, H.-P. & ECKELMANN, H. 1979 Propagation of perturbations in the viscous sublayer and adjacent wall region. *J. Fluid Mech.* **95**, 305–322.

KRISHNAMOORTHY, L. V. & ANTONIA, R. A. 1987 Temperature–dissipation measurements in a turbulent boundary layer. *J. Fluid Mech.* **176**, 265–281.

LU, S. S. & WILLMARTH, W. W. 1973 Measurements of the structure of the Reynolds stress in a turbulent boundary layer. *J. Fluid Mech.* **60**, 481–511.

LUCHIK, T. S. & TIEDERMAN, W. G. 1987 Timescale and structure of ejections and bursts in turbulent channel flow. *J. Fluid Mech.* **174**, 529–552.

MICHALKE, A. 1965 On spatially growing disturbances in an inviscid shear layer. *J. Fluid Mech.* **23**, 521–544.

MILLER, I. S., SHAH, D. A. & ANTONIA, R. A. 1987 A constant temperature hot wire anemometer. *J. Phys.* E: *Sci. Instrum.* **20**, 311–314.

NYCHAS, S. G., HERSHEY, H. C. & BRODKEY, R. S. 1973 A visual study of turbulent shear flow. *J. Fluid Mech.* **61**, 513–540.

OFFEN, G. R. & KLINE, S. J. 1975 A comparison and analysis of detection methods for the measurements of production in a boundary layer, *Proc. Third Biennial Symp. of Turbulence in Liquids, University of Missouri-Rolla*, pp. 289–320.

RANDOLPH, M., ECKELMANN, H. & NYCHAS, S. G. 1987 Identification of sweeps with the help of the instantaneous velocity gradient $\partial U/\partial y$. In *Advances in Turbulence* (ed. G. Comte-Bellot & J. Mathieu) pp. 408–415. Springer.

ROBINSON, S. K., KLINE, S. J. & SPALART, P. R. 1989 Quasi-coherent structures in the turbulent boundary layer. Part II: Verification and new information from a numerically simulated flat-plate layer. *Proc. Zaric Memorial Intl Seminar on Near-Wall Turbulence*. Hemisphere (to appear).

SHAH, D. A. & ANTONIA, R. A. 1989 Scaling of the 'bursting' period in turbulent boundary layer and duct flows. *Phys. Fluids* A, **1**, 318–325.

SMITH, C. R. & METZLER, S. P. 1983 The characteristics of low-speed streaks in the near-wall region of a turbulent boundary layer. *J. Fluid Mech.* **129**, 27–54.

SUBRAMANIAN, C. S., RAJAGOPALAN, S., ANTONIA, R. A. & CHAMBERS, A. J. 1982 Comparison of conditional sampling and averaging techniques in a turbulent boundary layer. *J. Fluid Mech.* **123**, 335–362.

TIEDERMAN, W. G. 1989 Eulerian detection of turbulent bursts. In *Proc. Zaric Memorial Intl Seminar on Near-Wall Turbulence*. Hemisphere (to appear).

WALLACE, J. M., BRODKEY, R. S. & ECKELMANN, H. 1977 Pattern-recognized structures in bounded turbulent shear flows. *J. Fluid Mech.* **83**, 673–693.

WALLACE, J. M., ECKELMANN, H. & BRODKEY, R. S. 1972 The wall region in turbulent shear flow. *J. Fluid Mech.* **54**, 39–48.

WILLMARTH, W. W. & SHARMA, L. K. 1984 Study of turbulent structure with hot wires smaller than the viscous length. *J. Fluid Mech.* **142**, 121–149.

ZARIC, Z., FALCO, R. E. & BLACKWELDER, R. F. 1984 Detection of coherent structures in visual and multiple hot-wire data in boundary layers. In *Turbulence and Chaotic Phenomena in Fluids* (ed. T. Tatsumi) pp. 439–445. North-Holland.